Form factor ratios for $B_s \to K\,\ell\,\nu$ and $B_s \to D_s\,\ell\,\nu$ semileptonic decays and $|V_{ub}/V_{cb}|$

Christopher J. Monahan,[1,*] Chris M. Bouchard,[2] G. Peter Lepage,[3] Heechang Na,[4] and Junko Shigemitsu[5]
(HPQCD Collaboration)

[1] *Institute for Nuclear Theory, University of Washington, Seattle, Washington 98195-1550, USA*
[2] *School of Physics and Astronomy, University of Glasgow, Glasgow G12 8QQ, United Kingdom*
[3] *Laboratory of Elementary Particle Physics, Cornell University, Ithaca, New York 14853, USA*
[4] *Ohio Supercomputer Center, 1224 Kinnear Road, Columbus, Ohio 43212, USA*
[5] *Department of Physics, The Ohio State University, Columbus, Ohio 43210, USA*

(Dated: December 21, 2018)

We present a lattice quantum chromodynamics determination of the ratio of the scalar and vector form factors for two semileptonic decays of the B_s meson: $B_s \to K\ell\nu$ and $B_s \to D_s\ell\nu$. In conjunction with future experimental data, our results for these correlated form factors will provide a new method to extract $|V_{ub}/V_{cb}|$, which may elucidate the current tension between exclusive and inclusive determinations of these Cabibbo-Kobayashi-Maskawa mixing matrix parameters. In addition to the form factor results, we determine the ratio of the differential decay rates, and forward-backward and polarization asymmetries, for the two decays.

I. INTRODUCTION

Semileptonic decays of heavy mesons provide stringent tests of the standard model of particle physics and opportunities to observe signals of new physics. In particular, experimental measurements of B decays have highlighted a number of deviations from standard model expectations. These discrepancies include $R(D^{(*)})$, the ratio of the branching fraction of the $B \to D^{(*)}\tau\nu$ and $B \to D^{(*)}e/\mu\nu$ decays, $R_{K^{(*)}}$, the ratio of the branching fraction of the $B \to K^{(*)}\mu^+\mu^-$ and $B \to K^{(*)}e^+e^-$ decays, and the long-standing tension between inclusive and exclusive determinations of the Cabibbo-Kobayashi-Maskawa (CKM) mixing matrix elements $|V_{ub}|$ and $|V_{cb}|$. Although none of these differences are conclusive evidence of new physics effects, the cumulative weight of these tensions suggest a hint of new physics.

The ratio $|V_{ub}/V_{cb}|$, which enters into the length of the side of the CKM unitarity triangle opposite the precisely-determined angle β, is a central input into tests of CKM unitarity. Both $|V_{ub}|$ and $|V_{cb}|$ have been determined through measurements of multiple exclusive mesonic decay channels [1, 2], primarily $B \to \pi\ell\overline{\nu}_\ell$ [3–11] and $B \to D^{(*)}\ell\overline{\nu}_\ell$ respectively [12–20], although other channels are also used [21–25]. The $B_s \to K$ decay has generally received less theoretical attention than the corresponding B decay, largely due to the absence of experimental data, although this channel has been studied on the lattice in [29**?**], and using other theoretical approaches [**?**], including light cone sum rules [**?** **?**], perturbative QCD [**?** **?**] and QCD-inspired models [**?** **?** **?** **?** **?**]. Form factors for both $B \to \pi\ell\overline{\nu}_\ell$ and $B \to D^{(*)}\ell\overline{\nu}_\ell$ decays have been calculated by several lattice groups [26–33] and using light cone sum rules [34–42], which provide complementary coverage of different kinematic regions. The leptonic decay $B \to \tau\overline{\nu}$ provides an alternative method to extract $|V_{ub}|$, but this approach is limited by current experimental uncertainties [1]. Most recently, the ratio $|V_{ub}/V_{cb}|$ was determined by the LHCb collaboration through the ratio of the baryonic decays $\Lambda_b^0 \to \Lambda_c^+\mu\overline{\nu}$ and $\Lambda_b^0 \to p\mu\overline{\nu}$ [43, 44], using form factors determined with lattice QCD [45]. Inclusive determinations of $|V_{ub}|$ differ from the value extracted from exclusive decays at the level of approximately three standard deviations.

Here we undertake a correlated study of the form factors for the $B_s \to K\ell\overline{\nu}_\ell$ and $B_s \to D_s\ell\overline{\nu}_\ell$ decays, which, in conjunction with anticipated experimental results from the LHCb Collaboration, will provide a new method to determine the ratio $|V_{ub}/V_{cb}|$. We perform a chiral-continuum-kinematic fit to the scalar and vector form factors for both the $B_s \to K\ell\overline{\nu}_\ell$ [46] and $B_s \to D_s\ell\overline{\nu}_\ell$ decays [47], to determine the correlated form factors over the full range of momentum transfer. Using the ratio of the form factors significantly reduces the largest systematic uncertainty at large values of the momentum transfer, which stems from the perturbative matching of lattice nonrelativistic QCD (NRQCD) currents to continuum QCD. We use our form factor results to predict several phenomenological ratios, including the differential branching fractions, and the forward-backward and polarization asymmetries.

We briefly summarize the details of the lattice calculations used in the analyses of [46, 47] in Sec. II and the corresponding form factor results in Sec. III. We then present our new chiral-continuum-kinematic extrapolation in Sec. IV, and our phenomenological predictions in Sec. V, before summarizing in Sec. VI. We provide further details of the input two-point correlator data in Appendix A and details required to reconstruct our chiral-continuum-kinematic fit in Appendix B.

* e-mail: cjm373@uw.edu

TABLE I. Details of three "coarse" and two "fine" $n_f = 2+1$ MILC ensembles used in the determination of the scalar and vector form factors.

Set	r_1/a	m_l/m_s (sea)	$N_{\rm conf}$ (K/D_s)	$N_{\rm tsrc}$	$L^3 \times N_t$
C1	2.647	0.005/0.050	1200/2096	2/4	$24^3 \times 64$
C2	2.618	0.010/0.050	1200/2256	2/2	$20^3 \times 64$
C3	2.644	0.020/0.050	600/1200	2/2	$20^3 \times 64$
F1	3.699	0.0062/0.031	1200/1896	4/4	$28^3 \times 96$
F2	3.712	0.0124/0.031	600/1200	4/4	$28^3 \times 96$

II. ENSEMBLES, CURRENTS AND CORRELATORS

Our determination of the ratio of the form factors for the exclusive $B_s \to X_s \ell\nu$ semileptonic decays closely parallels the analyses presented in [31, 46, 47]. Throughout this work, we use X_s to represent a K or D_s meson. We use the two- and three-point correlator data presented in [46, 47] to perform a simultaneous, correlated fit of the form factors for both $B_s \to K\ell\nu$ and $B_s \to D_s\ell\nu$ decays. In this section we outline the details of the ensembles, reproduce the form factor results for convenience, and refer the reader to [31, 46, 47] for details of the correlator analysis.

We use five gauge ensembles with $n_f = 2+1$ flavors of AsqTad sea quarks generated by the MILC Collaboration [48], including three "coarse" (with lattice spacing $a \approx 0.12\,\text{fm}$) and two "fine" (with $a \approx 0.09\,\text{fm}$) ensembles. We summarize these ensembles in Table I and tabulate the corresponding light pseudoscalar masses, for both AsqTad and HISQ valence quarks, in Table II.

In Table III we list the valence quark masses for the NRQCD bottom quarks and HISQ charm quarks [46, 50]. For completeness and ease of reference, we include both the tree-level wave function renormalization for the massive HISQ quarks [51] and the spin-averaged Υ mass, corrected for electroweak effects, determined in [50].

The scalar, $f_0^{(X_s)}(q^2)$, and vector, $f_+^{(X_s)}(q^2)$, form factors that characterize the $B_s \to X_s$ semileptonic decays are defined by the matrix element

$$\langle X_s(p_{X_s})|V^\mu|B_s(p_{B_s})\rangle = f_0^{(X_s)}(q^2)\frac{M_{B_s}^2 - M_{X_s}^2}{q^2}q^\mu + f_+^{X_s}(q^2)\left[p_{B_s}^\mu + p_{X_s}^\mu - \frac{M_{B_s}^2 - M_{X_s}^2}{q^2}q^\mu\right], \quad (1)$$

where V^μ is a flavor-changing vector current and the momentum transfer is $q^\mu = p_{B_s}^\mu - p_{X_s}^\mu$. On the lattice it is more convenient to work with the form factors $f_\parallel^{(X_s)}$ and $f_\perp^{(X_s)}$, which are given in terms of the scalar and vector form factors by

$$f_+^{(X_s)}(q^2) = \frac{1}{\sqrt{2M_{B_s}}}\Big[f_\parallel^{(X_s)}(q^2) + (M_{B_s} - E_{X_s})f_\perp^{(X_s)}(q^2)\Big], \quad (2)$$

$$f_0^{(X_s)}(q^2) = \frac{\sqrt{2M_{B_s}}}{M_{B_s}^2 - M_{X_s}^2}\Big[(M_{B_s} - E_{X_s})f_\parallel^{(X_s)}(q^2) + (E_{X_s}^2 - M_{X_s}^2)f_\perp^{(X_s)}(q^2)\Big]. \quad (3)$$

Here E_{X_s} is the energy of the X_s meson in the rest frame of the B_s meson. We work in the rest frame of the B_s meson and throughout the rest of this work the spatial momentum, $\vec{p}$, denotes the momentum of the X_s meson.

NRQCD is an effective theory for heavy quarks and results determined using lattice NRQCD must be matched to full QCD to make contact with experimental data. We match the bottom-charm currents, J_μ, at one loop in perturbation theory through $\mathcal{O}(\alpha_s, \Lambda_{\rm QCD}/m_b, \alpha_s/(am_b))$, where am_b is the bare lattice mass [51]. We rescale all currents by the nontrivial massive wave function renormalization for the HISQ charm quarks, tabulated in Table III, and taken from [31, 51].

The B_s and X_s meson two-point correlators and three-point correlators of the NRQCD-HISQ currents, J_μ, were calculated in [46, 47]. In those calculations, we used smeared heavy-strange bilinears to represent the B_s meson and incorporated both delta-function and Gaussian smearing, with a smearing radius of $r_0/a = 5$ and $r_0/a = 7$ on the coarse and fine ensembles, respectively. The three-point correlators were determined with the setup illustrated in Fig. 1. The B_s meson is created at time t_0 and a current J_μ inserted at time t, between t_0 and $t_0 + T$. The X_s meson is then annihilated at time $t_0 + T$. We used four values of T: 12, 13, 14, and 15 on the coarse lattices; and 21, 22, 23, and 24 on the fine lattices. We implemented spatial sums at the source through the $U(1)$ random wall sources $\xi(x)$ and $\xi(x')$ [52] and generated data for four different values of the X_s meson momenta, $\vec{p} = 2\pi/(aL)(0,0,0)$, $\vec{p} = 2\pi/(aL)(1,0,0)$, $\vec{p} = 2\pi/(aL)(1,1,0)$, and $\vec{p} = 2\pi/(aL)(1,1,1)$, where L is the spatial lattice extent.

III. CORRELATOR AND FORM FACTOR RESULTS

The results for the two- and three-point correlators were determined with a Bayesian multiexponential fitting procedure, based on the `PYTHON` packages `LSQFIT` [53] and `CORRFITTER` [54]. The results are summarized for convenience in Appendix A.

We summarize the final results for the form factors, $f_0(\vec{p})$ and $f_+(\vec{p})$, for each ensemble and X_s momentum in Tables IV and V. For more details, see [31, 46, 47].

TABLE II. Light meson masses on MILC ensembles for both AsqTad [48] and HISQ valence quarks [46]. In the final column we list the finite volume corrections to chiral logarithms from staggered perturbation theory [49], for each ensemble.

Set	$aM_\pi^{\rm AsqTad}$	$aM_\pi^{\rm HISQ}$	$aM_K^{\rm AsqTad}$	$aM_K^{\rm HISQ}$	$aM_{\eta_s}^{\rm HISQ}$	$aM_{D_s}^{\rm HISQ}$	$\delta_{\rm FV}$
C1	0.15971(20)	0.15990(20)	0.36530(29)	0.31217(20)	0.41111(12)	1.18755(22)	0.053647
C2	0.22447(17)	0.21110(20)	0.38331(24)	0.32851(48)	0.41445(17)	1.20090(30)	0.030760
C3	0.31125(16)	0.29310(20)	0.40984(21)	0.35720(22)	0.41180(23)	1.19010(33)	0.003375
F1	0.14789(18)	0.13460(10)	0.25318(19)	0.22855(17)	0.294109(93)	0.84674(12)	0.059389
F2	0.20635(18)	0.18730(10)	0.27217(21)	0.24596(14)	0.29315(12)	0.84415(14)	0.007567

TABLE III. Valence quark masses am_b for NRQCD bottom quarks and am_s and am_c for HISQ strange and charm quarks. The fifth column gives $Z_2^{(0)}(am_c)$, the tree-level wave function renormalization constant for massive (charm) HISQ quarks. The sixth column lists the values of the spin-averaged Υ mass, corrected for electroweak effects.

Set	am_b	am_s	am_c	$Z_2^{(0)}(am_c)$	$aE_{b\bar{b}}^{\rm sim}$
C1	2.650	0.0489	0.6207	1.00495618	0.28356(15)
C2	2.688	0.0492	0.6300	1.00524023	0.28323(18)
C3	2.650	0.0491	0.6235	1.00504054	0.27897(20)
F1	1.832	0.0337	0.4130	1.00103879	0.25653(14)
F2	1.826	0.0336	0.4120	1.00102902	0.25558(28)

FIG. 1. Lattice setup for the three-point correlators. See accompanying text for details.

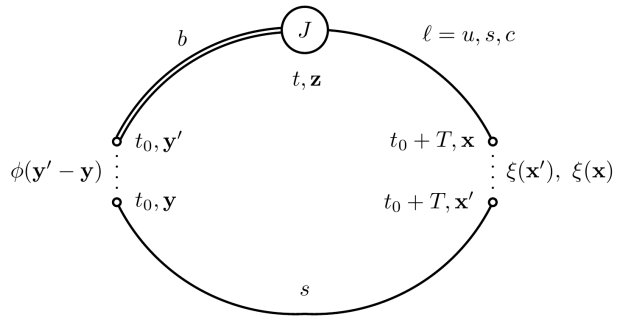

IV. CHIRAL, CONTINUUM AND KINEMATIC EXTRAPOLATIONS

Form factors determined from experimental data are functions of a single kinematic variable, which is typically the momentum transfer, q^2, or the energy of the mesonic decay product, E_{X_s}. Alternatively, the form factors can be expressed in terms of the z-variable,

$$z(q^2) = \frac{\sqrt{t_+ - q^2} - \sqrt{t_+ - t_0}}{\sqrt{t_+ - q^2} + \sqrt{t_+ - t_0}}. \tag{4}$$

Here $t_+ = (M_{B_s} + M_{X_s})^2$ and t_0 is a free parameter, which we take to be $t_0 = (M_{B_s} + M_{X_s})(\sqrt{M_{B_s}} + \sqrt{M_{X_s}})^2$, as in [46]. This choice minimizes the magnitude of z over the physical range of momentum transfer. Note that in [47] the choice $t_0 = q^2_{\rm max} = (M_{B_s} - M_{X_s})^2$ was used to ensure consistency with the analysis of [31]. We have confirmed that our extrapolation results are independent of our choice of t_0, within fit uncertainties.

Lattice calculations of form factors are necessarily determined at finite lattice spacing, generally with light quark masses that are heavier than their physical values, and are thus functions of the lattice spacing and the light quark mass in addition to the momentum transfer. We remove the lattice spacing and light quark mass dependence of the lattice results by performing a combined continuum-chiral-kinematic extrapolation, through the modified z-expansion, which was introduced in [52, 55] and applied to B_s semileptonic decays in [46, 47, 56, 57].

Our chiral-continuum-kinematic extrapolation for the $B_s \to X_s \ell \nu$ decays closely parallels those studied in [31, 46, 47], so here we outline the main components and refer the reader to those references for details.

The dependence of the form factors on the z-variable is expressed through a modification of the Bourrely-Caprini-Lellouch (BCL) parametrization [58]

$$P_0^{(X_s)} f_0^{(X_s)}(q^2(z)) = \left[1 + L^{(X_s)}\right] \times \sum_{j=0}^{J-1} a_j^{(0,X_s)}(m_l, m_l^{\rm sea}, a) z^j, \tag{5}$$

$$P_+^{(X_s)} f_+^{(X_s)}(q^2(z)) = \left[1 + L^{(X_s)}\right] \times \sum_{j=0}^{J-1} a_j^{(+,X_s)}(m_l, m_l^{\rm sea}, a) \left[z^j - (-1)^{j-J} \frac{j}{J} z^J\right]. \tag{6}$$

Here the $P_{0,+}$ are Blaschke factors that take into account the effects of expected poles above the physical region,

$$P_{0,+}^{(X_s)}(q^2) = \left(1 - \frac{q^2}{\left(M_{0,+}^{(X_s)}\right)^2}\right), \tag{7}$$

where we take [46, 47, 59]

$$M_+^{(K)} = 5.325\,20(48)\,{\rm GeV}, \tag{8}$$

$$M_0^{(K)} = 5.6794(10)\,{\rm GeV}, \tag{9}$$

$$M_+^{(D_s)} = M_{B_c^*} = 6.330(9)\,{\rm GeV}, \tag{10}$$

$$M_0^{(D_s)} = 6.42(10)\,{\rm GeV}. \tag{11}$$

TABLE IV. Final results for the form factors $f_0^{(K)}(\vec{p})$ and $f_+^{(K)}(\vec{p})$. Data reproduced from Table II of [46].

Set	$f_0^{(K)}(0,0,0)$	$f_0^{(K)}(1,0,0)$	$f_0^{(K)}(1,1,0)$	$f_0^{(K)}(1,1,1)$	$f_+^{(K)}(1,0,0)$	$f_+^{(K)}(1,1,0)$	$f_+^{(K)}(1,1,1)$
C1	0.8244(23)	0.7081(27)	0.6383(30)	0.5938(41)	2.087(16)	1.657(14)	1.378(13)
C2	0.8427(25)	0.6927(35)	0.6036(49)	0.536(12)	1.880(12)	1.412(16)	1.142(33)
C3	0.8313(29)	0.6953(33)	0.6309(30)	0.5844(46)	1.773(11)	1.4212(84)	1.184(10)
F1	0.8322(25)	0.6844(35)	0.5994(43)	0.5551(56)	1.878(13)	1.385(12)	1.158(13)
F2	0.8316(27)	0.6915(38)	0.6199(43)	0.5563(61)	1.834(14)	1.396(10)	1.163(14)

TABLE V. Final results for the form factors $f_0^{(D_s)}(\vec{p})$ and $f_+^{(D_s)}(\vec{p})$. Data reproduced from Tables VI and VII of [47].

Set	$f_0^{(D_s)}(0,0,0)$	$f_0^{(D_s)}(1,0,0)$	$f_0^{(D_s)}(1,1,0)$	$f_0^{(D_s)}(1,1,1)$	$f_+^{(D_s)}(1,0,0)$	$f_+^{(D_s)}(1,1,0)$	$f_+^{(D_s)}(1,1,1)$
C1	0.8885(11)	0.8754(14)	0.8645(13)	0.8568(13)	1.1384(35)	1.1081(20)	1.0827(21)
C2	0.8822(13)	0.8663(15)	0.8524(16)	0.8418(18)	1.1137(29)	1.0795(22)	1.0470(21)
C3	0.8883(13)	0.8723(16)	0.8603(16)	0.8484(21)	1.1260(34)	1.0912(24)	1.0552(28)
F1	0.90632(98)	0.8848(13)	0.8674(13)	0.8506(17)	1.1453(29)	1.0955(24)	1.0549(24)
F2	0.9047(12)	0.8855(16)	0.8667(15)	0.8487(19)	1.1347(42)	1.0905(26)	1.0457(33)

In line with [46], we convert these values to lattice units in the chiral-continuum-kinematic extrapolation, so that the difference between the ground state meson masses and these pole masses is fixed in physical units.

The functions $L^{(X_s)}$ incorporate the chiral logarithmic corrections, which are fixed by hard pion chiral perturbation theory [60, 61] for the $B_s \to K$ decay

$$L^K = -\frac{3}{8}x_\pi(\log x_\pi + \delta_{\rm FV}) - \frac{1+6g^2}{4}x_K \log x_K - \frac{1+12g^2}{24}x_\eta \log x_\eta. \quad (12)$$

Here $g^2 = 0.51(20)$, $\delta_{\rm FV}$ are finite volume corrections given in Table II, we define

$$x_{\pi,K,\eta,\eta_s} = \frac{M^2_{\pi,K,\eta,\eta_s}}{(4\pi f_\pi)^2}, \quad (13)$$

$$\delta x_{\pi,K} = \frac{(M^{\rm AsqTad}_{\pi,K})^2 - (M^{\rm HISQ}_{\pi,K})^2}{(4\pi f_\pi)^2}, \quad (14)$$

$$\delta x_{\eta_s} = \frac{(M^{\rm HISQ}_{\eta_s})^2 - (M^{\rm phys.}_{\eta_s})^2}{(4\pi f_\pi)^2}, \quad (15)$$

and $M^2_\eta = (M^2_\pi + 2M^2_{\eta_s})/3$. We tabulate the meson masses required to calculate $\delta x_{\pi,K,\eta_s}$ in Table II. For the $B_s \to D_s$ decay, the chiral logarithmic corrections cannot be factored out in the z-expansion [61] and therefore we follow [31, 47] and fit the logarithmic dependence by introducing corresponding fit parameters in the expansion coefficients $a_j^{(0,+,D_s)}$. In other words, we take

$$L^{(D_s)} = 0, \quad (16)$$

and introduce an appropriate fit parameter, $c_j^{(2)}$, in the corresponding fit function, Eq. (19).

The expansion coefficients $a_j^{(0,+,X_s)}$ include lattice spacing and quark mass dependence and can be written as

$$a_j^{(0,+,X_s)}(m_l, m_l^{\rm sea}, a) = \widetilde{a}_j^{(0,+,X_s)} \widetilde{D}_j^{(0,+,X_s)}(m_l, m_l^{\rm sea}, a), \quad (17)$$

where the $\widetilde{D}_j^{(0,+,X_s)}$ include all lattice artifacts. Suppressing the $0,+$ superscripts for clarity, these coefficients are given by [46]

$$\widetilde{D}_j^{(K)} = 1 + c_j^{(1)}x_\pi + d_j^{(1)}\left(\frac{\delta x_\pi}{2} + \delta x_K\right) + d_j^{(2)}\delta x_{\eta_s} + e_j^{(1)}\left(\frac{aE_K}{\pi}\right)^2 + e_j^{(2)}\left(\frac{aE_K}{\pi}\right)^4 + f_j^{(1)}\left(\frac{a}{r_1}\right)^2 + f_j^{(2)}\left(\frac{a}{r_1}\right)^4, \quad (18)$$

and [47]

$$\widetilde{D}_j^{(D_s)} = 1 + c_j^{(1)}x_\pi + c_j^{(2)}x_\pi\log(x_\pi) + d_j^{(1)}\left(\frac{\delta x_\pi}{2} + \delta x_K\right) + d_j^{(2)}\delta x_{\eta_s} + e_j^{(1)}\left(\frac{aE_{D_s}}{\pi}\right)^2 + e_j^{(2)}\left(\frac{aE_{D_s}}{\pi}\right)^4 + m_j^{(1)}(am_c)^2 + m_j^{(2)}(am_c)^4. \quad (19)$$

Here the $c_j^{(i)}$, $d_j^{(i)}$, $e_j^{(i)}$, $f_j^{(i)}$, and $m_j^{(i)}$ are fit parameters, along with the $\widetilde{a}_j^{(0,+)}$. We incorporate light- and heavy-quark mass dependence in the discretization coefficients $f_j^{(i)}$ by replacing

$$f_j^{(i)} \to f_j^{(i)}(1 + l_j^{(1,i)}x_\pi + l_j^{(2,i)}x_\pi^2) \times (1 + h_j^{(1,i)}\delta m_b + h_j^{(2,i)}(\delta m_b)^2), \quad (20)$$

where $\delta m_b = am_b - 2.26$ [46] and is chosen to minimize the magnitude of δm_b, such that $-0.4 < \delta m_b < 0.4$. Here

x_π captures sea pion mass dependence and is determined from the AsqTad pion mass [48].

The actions we use are highly improved and $\mathcal{O}(a^2)$ tree-level lattice artifacts have been removed. The $\mathcal{O}(\alpha_s a^2)$ and $\mathcal{O}(a^4)$ corrections are dominated by powers of (am_c) and (aE_{X_s}), rather than those of the spatial momenta (ap_i). Thus, we do not incorporate terms involving hypercubic invariants constructed from the spatial momentum ap_i [62].

We follow [46, 47] and impose the kinematic constraint $f_0(0) = f_+(0)$ analytically for the $B_s \to K$ decay, and as a data point for the $B_s \to D_s$ channel. To incorporate the systematic uncertainty associated with truncation of the perturbative current-matching procedure at $\mathcal{O}(\alpha_s, \Lambda_{\rm QCD}/m_b, \alpha_s/(am_b))$, we introduce fit parameters $m_\parallel$ and $m_\perp$, with central value zero and width $\delta m_{\parallel,\perp}$ and re-scale the form factors, $f_\parallel$ and $f_\perp$ according to

$$f_{\parallel,\perp} \to (1 + m_{\parallel,\perp}) f_{\parallel,\perp}. \tag{21}$$

We take $\delta m_{\parallel,\perp} = 0.04$. We refer to this fit Ansatz, including terms up to z^3 in the modified z-expansion, as the "standard extrapolation."

To test the convergence of our fit Ansatz and ensure we have included a sufficient number of terms in the modified z-expansion, we modify the fit Ansatz in the following ways:

1. include terms up to z^2 in the z-expansion;
2. include terms up to z^4 in the z-expansion;
3. include discretization terms up to $(am_c)^2$;
4. include discretization terms up to $(am_c)^6$;
5. include discretization terms up to $(a/r_1)^2$;
6. include discretization terms up to $(a/r_1)^6$;
7. include discretization terms up to $(aE_K/\pi)^2$;
8. include discretization terms up to $(aE_K/\pi)^6$;
9. include discretization terms up to $(aE_{D_s}/\pi)^2$;
10. include discretization terms up to $(aE_{D_s}/\pi)^6$;

We show the results of these modifications in Fig. 2, where we label the standard fit Ansatz as "Test 0". These tests demonstrate the stability of the standard fit Ansatz; adding higher order terms does not alter the fit results or improve the goodness-of-fit.

We also study the stability of the fit with respect to the following variations:

i. omit the $x_\pi \log(x_\pi)$ term;

ii. omit the light quark mass-dependent discretization terms from the $f_j^{(i)}$ coefficients;

iii. add strange quark mass-dependent discretization terms to the $f_j^{(i)}$ coefficients;

FIG. 2. Comparison of the convergence tests of the "standard extrapolation" fit Ansatz. The top panel shows the χ^2/dof for each test, normalized by the χ^2/dof for the standard extrapolation. The lower panel shows the fit results for the form factor ratio $f_0^{(K)}/f_0^{(D_s)}$ at $q^2 = 0$. The test numbers labeling the horizontal axis correspond to the modifications listed in the text. The first data point, the purple square, is the "standard extrapolation" fit result, which is also represented by the purple shaded band.

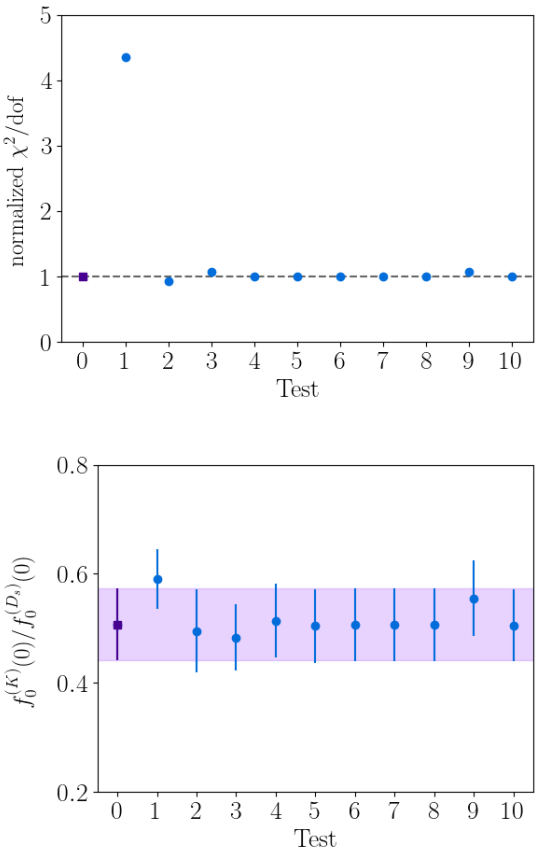

iv. omit the am_b-dependent discretization terms from the $f_j^{(i)}$ coefficients;

v. omit sea- and valence-quark mass difference, $d_j^{(1)}$;

vi. omit the strange quark mass mistuning, $d_j^{(2)}$;

vii. omit finite volume effects;

viii. add light-quark mass dependence to the $m_j^{(i)}$ fit parameters;

ix. add strange-quark mass dependence to the $m_j^{(i)}$ fit parameters;

x. add bottom-quark mass dependence to the $m_j^{(i)}$ fit parameters;

FIG. 3. Analogous to Fig. 2, but for stability tests labeled by "i." to "xii." in the text. Details provided in the caption of Fig. 2.

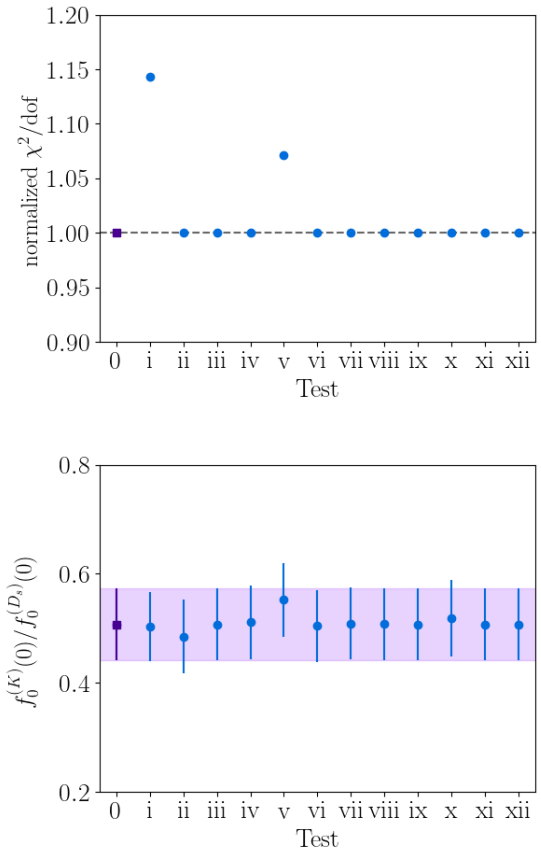

xi. incorporate a 2% uncertainty for higher-order matching contributions;

xii. incorporate a 5% uncertainty for higher-order matching contributions;

We show the results of these stability tests in Fig. 3. Test 0 represents the standard fit Ansatz. Taken together, these plots demonstrate that the fit has converged with respect to a variety of modifications of the chiral-continuum-kinematic extrapolation Ansatz.

V. RESULTS

A. Form factor ratios

Our final results, from a simultaneous fit to both decay channels, for the ratio of form factors at zero momentum transfer are

$$\frac{f_0^{(K)}(0)}{f_0^{(D_s)}(0)} = 0.507(66), \tag{22}$$

where the uncertainties account for correlations between the form factor results for each decay channel. The corresponding results for the individual form factors at zero momentum transfer are $f_0^{(K)}(0) = 0.341(42)$ and $f_0^{(D_s)}(0) = 0.661(42)$, in good agreement with the results of [46] and [47], respectively. The result in Eq. (22) is in good agreement with, but with significantly reduced uncertainties, the value obtained assuming uncorrelated uncertainties between the results of [46, 47]: $f_0^{(K)}(0)/f_0^{(D_s)}(0) = 0.323(63)/0.656(31) = 0.492(99)$.

We obtain a reduced χ^2 of $\chi^2/\text{dof} = 1.3$ with 71 degrees of freedom (dof), with a quality factor of $Q = 0.011$. The Q-value (or p-value) corresponds to the probability that the χ^2/dof from the fit could have been larger, by chance, assuming the data are all Gaussian and consistent with each other. The simultaneous fit ensures that the uncertainties associated with the perturbative matching procedure for the heavy-light currents largely cancel in the form factor ratio. This can be seen by comparing the error budget contribution from perturbative matching in Table VI, with the individual fits, for which the perturbative truncation uncertainty was the second-largest source of uncertainty. The uncertainties in our ratio results are dominated by the $B_s \to K$ channel, which has fewer statistics and a larger extrapolation uncertainty, because, in the region of momentum transfer reported here, $0 - -12.5$ GeV^2, the corresponding form factors are extrapolated further from the region in which we have lattice results.

We tabulate our choice of priors and the fit results in the Appendix, where we provide the corresponding z-expansion coefficients and their correlations. Following [47], based on the earlier work of [31, 52, 55], we split the priors into three groups. Broadly speaking, Group I priors includes the typical fit parameters, Group II the input lattice scales and masses, and Group III priors the inputs from experiment, such as physical meson masses. We plot our final results for the ratios of the form factors, $f_0^{(K)}/f_0^{(D_s)}(q^2)$ and $f_+^{(K)}/f_+^{(D_s)}(q^2)$, as a function of the momentum transfer, q^2, in Fig. 4. Details required to reconstruct the fully correlated form factors are given in Appendix B.

B. Form factor error budget

We tabulate the errors in the ratios of the form factors at zero momentum transfer, Eq. (22), in Table VI. The sources of uncertainty listed in Table VI are:

a. Statistical. Statistical uncertainties include the two- and three-point correlator fit errors and those associated with the lattice spacing determination, r_1 and r_1/a. These effects are the second largest source of uncertainty in our results, and are dominated by the smaller statistics available in the $B_s \to K$ analysis.

b. Chiral extrapolation. Includes the uncertainties arising from extrapolation in both valence and sea quark

FIG. 4. Chiral and continuum extrapolated form factor ratios, $f_0^{(K)}/f_0^{(D_s)}(q^2)$ (upper panel) and $f_+^{(K)}/f_+^{(D_s)}(q^2)$ (lower panel), as a function of the momentum transfer, q^2. The dashed lines indicate the central values of the extrapolated form factors and the uncertainty bands include all sources of statistical and systematic uncertainty.

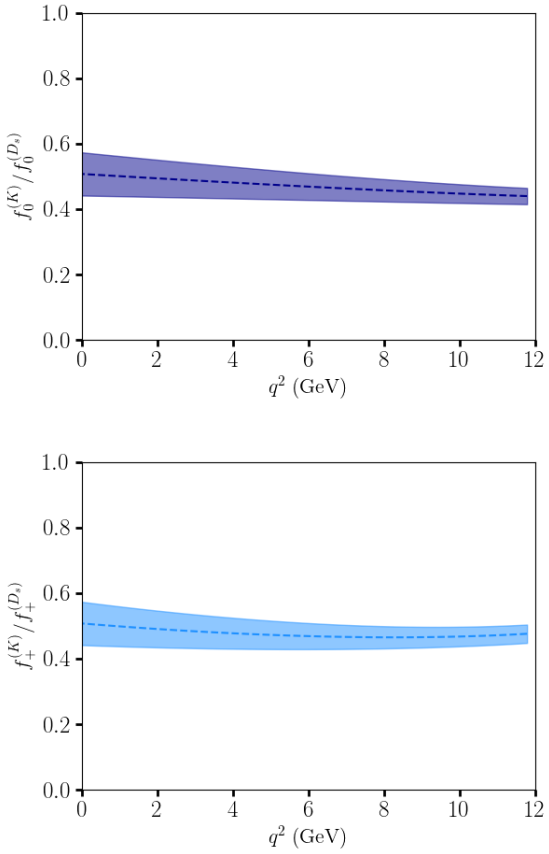

TABLE VI. Error budget for the form factor ratios at zero momentum transfer, Eq. (22). We describe each source of uncertainty in more detail in the accompanying text.

Type	Partial uncertainty (%)
Statistical	6.63
Chiral extrapolation	0.89
Quark mass tuning	2.18
Discretization	4.16
Kinematic	9.31
Matching	0.28
Total	13.03

masses and from the $B_s \to D_s$ chiral logarithms in the chiral-continuum extrapolation, corresponding to the fit parameters $c_j^{(i)}$ in Eqs. (18) and (19).

c. Quark mass tuning. These uncertainties arise from tuning the light and strange quark masses at finite lattice spacing and partial quenching effects.

d. Discretization. These effects include the $(aE_{X_s}/\pi)^n$, $(a/r_1)^n$, and $(am_c)^n$ terms in the modified z-expansion, corresponding to the fit parameters $e_j^{(i)}$, $f_j^{(i)}$ and $m_j^{(i)}$ in Eqs. (18) and (19).

e. Kinematic. Uncertainties that arise from the z-expansion coefficients, including the Blaschke factors. These effects are the dominant source of uncertainty in our results, and again predominantly arise from the $B_s \to K$ channel.

f. Matching. The perturbative matching uncertainties stemming from the truncation of the expansion of NRQCD-HISQ effective currents in terms of QCD currents. These are the second largest source of uncertainty in the results for the individual channels, but the effects largely cancel in the ratio. This is further demonstrated by tests (xi) and (xii) of the previous section, in which changing the matching uncertainty from 2% to 5% has practically negligible effect on the fit, and in particular, the ratio at zero momentum transfer.

We propagate all uncertainties from the large momentum-transfer region, for which we have lattice results, to zero momentum transfer. We do not include the uncertainties associated with physical meson mass input errors and finite volume effects, which are both less than 0.01%, because they are negligible contributions to our error budget estimates. Moreover, we neglect uncertainties from isospin breaking, electromagnetic effects, and charm-quark quenching effects in the gauge ensembles.

We plot our estimated error budges for the ratios of the form factors, $f_0(q^2)$ and $f_+(q^2)$, as a function of the momentum transfer, q^2, in Fig. 5.

C. Semileptonic decay phenomenology

The experimental measurements of the ratio

$$R(D) = \frac{\mathcal{B}(B \to D\tau\nu)}{\mathcal{B}(B \to D\ell\nu)}, \tag{23}$$

which measures the ratio of branching fraction of the semileptonic decay to the τ lepton to the branching fraction to an electron or muon (represented by ℓ), are currently in tension with the standard model result. The global experimental average is [63–66]

$$R(D)_{\text{exp.}} = 0.391(41)_{\text{stat.}}(28)_{\text{sys.}}, \tag{24}$$

whereas the standard model expectation, neglecting correlations between the calculations [31, 67, 68], is

$$R(D)_{\text{theor.}} = 0.299(7). \tag{25}$$

We determine the corresponding ratio of the R-ratios for the semileptonic $B_s \to X_s\ell\nu$ decays,

$$\frac{R(K)}{R(D_s)} = 2.02(12), \tag{26}$$

FIG. 5. Error budget estimates for the ratios of the form factors, $f_0^{(K)}/f_0^{(D_s)}(q^2)$ (upper panel) and $f_+^{(K)}/f_+^{(D_s)}(q^2)$ (lower panel), as a function of the momentum transfer, q^2.

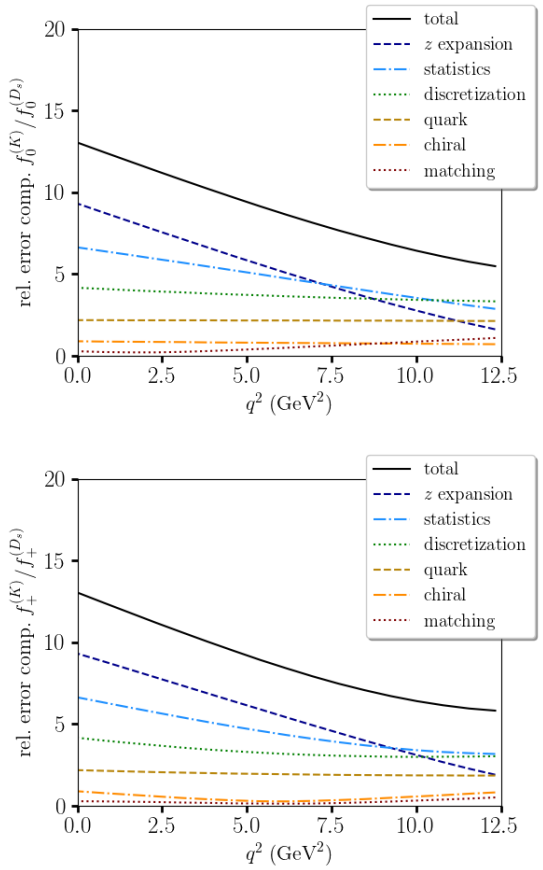

which is in agreement with, but with slightly smaller errors than, the value of $R(K)/R(D_s) = 0.695(50)/0.314(6) = 2.21(16)$ obtained assuming uncorrelated uncertainties between the values given in [46, 47].

Neglecting final state electromagnetic interactions, the full angular dependence of the differential decay rate for $B_s \to X_s \ell\nu$ is given in terms of the corresponding scalar and vector form factors by

$$\begin{aligned}\frac{\mathrm{d}^2\Gamma(B_s \to X_s\ell\nu)}{\mathrm{d}q^2\,\mathrm{d}\cos\theta_\ell} &= \frac{G_F^2|V_{xb}|^2}{128\pi^3 M_{B_s}}\left(1-\frac{m_\ell^2}{q^2}\right)^2 |\vec{p}_{X_s}| \\ &\times\Bigg[4M_{B_s}^2\vec{p}_{X_s}^{\,2}\left(\sin^2\theta_\ell + \frac{m_\ell^2}{q^2}\cos^2\theta_\ell\right)|f_+|^2 \\ &+\frac{4m_\ell^2}{q^2}\left(M_{B_s}^2 - M_{X_s}^2\right)M_{B_s}|\vec{p}_{X_s}|\cos\theta_\ell f_0 f_+ \\ &+\frac{m_\ell^2}{q^2}\left(M_{B_s}^2 - M_{X_s}^2\right)^2|f_0|^2\Bigg]. \end{aligned} \quad (27)$$

Here θ_ℓ is defined as the angle between the final state lepton and the B_s meson, in the frame in which $\vec{p}_\ell + \vec{p}_\nu = \vec{0}$. Integrating over the angle θ_ℓ, one obtains the standard

FIG. 6. Ratio of the differential decay rates, $\gamma_\ell^{(K)}/\gamma_\ell^{(D_s)}$, divided by $|V_{ub}/V_{cb}|^2$, as a function of the momentum transfer, q^2.

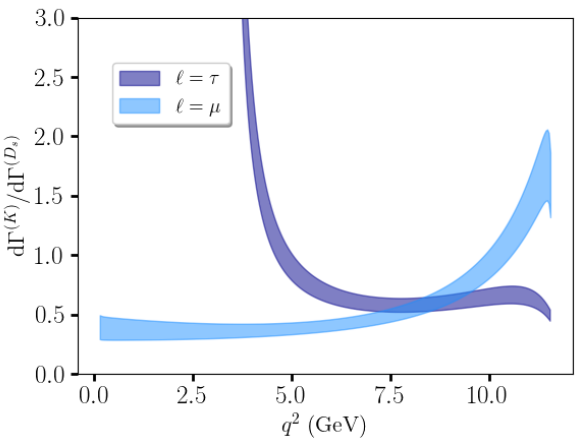

model differential decay rate,

$$\begin{aligned}\gamma_\ell^{(X_s)} &= \frac{\mathrm{d}^2\Gamma(B_s \to X_s\ell\nu)}{\mathrm{d}q^2} \\ &= \frac{G_F^2|V_{xb}|^2}{24\pi^3 M_{B_s}}\left(1-\frac{m_\ell^2}{q^2}\right)^2 |\vec{p}_{X_s}| \\ &\times\left[\left(1+\frac{m_\ell^2}{2q^2}\right)M_{B_s}^2\vec{p}_{X_s}^{\,2}|f_+|^2\right. \\ &\left.+\frac{3m_\ell^2}{8q^2}\left(M_{B_s}^2 - M_{X_s}^2\right)^2|f_0|^2\right]. \end{aligned} \quad (28)$$

In Fig. 6 we plot the ratio of the differential decay rates, $\gamma_\ell^{(K)}/\gamma_\ell^{(D_s)}$, as a function of the momentum transfer, for the semileptonic decays to muons ($\ell = \mu$) and to tau leptons ($\ell = \tau$).

We combine our results for these decay rate ratios with the experimental world average results for $|V_{ub}/V_{cb}|$ [1], using both inclusive and exclusive determinations,

$$\text{exclusive } |V_{ub}/V_{cb}| = 0.088(6), \quad (29)$$
$$\text{inclusive } |V_{ub}/V_{cb}| = 0.107(7), \quad (30)$$

and plot the results in Fig. 7. The LHCb Collaboration has measured this ratio to be $|V_{ub}/V_{cb}| = 0.083(6)$, updated in [1] to $|V_{ub}/V_{cb}| = 0.080(6)$, from the ratio of the baryonic semileptonic decays $\Lambda_b \to p^+\mu^-\overline{\nu}$ and $\Lambda_b \to \Lambda_c^+\mu^-\overline{\nu}$ [43]. This result is sufficiently close to the world average given in Eqs. (29) that we do not include it in Fig. 7. A correlated average, $|V_{ub}/V_{cb}| = 0.092(8)$, of both inclusive and exclusive results is given in [1], which also includes the experimental result from baryonic decays, but the large discrepancy between the inclusive and exclusive determinations suggests that this average should be treated with caution.

FIG. 7. Ratio of the differential decay rates, $\gamma_\ell^{(K)}/\gamma_\ell^{(D_s)}$, using inclusive and exclusive world average results for $|V_{ub}/V_{cb}|$, as a function of the momentum transfer, q^2. The upper panel shows the decay rates for $\ell = \tau$, and the lower panel $\ell = \mu$.

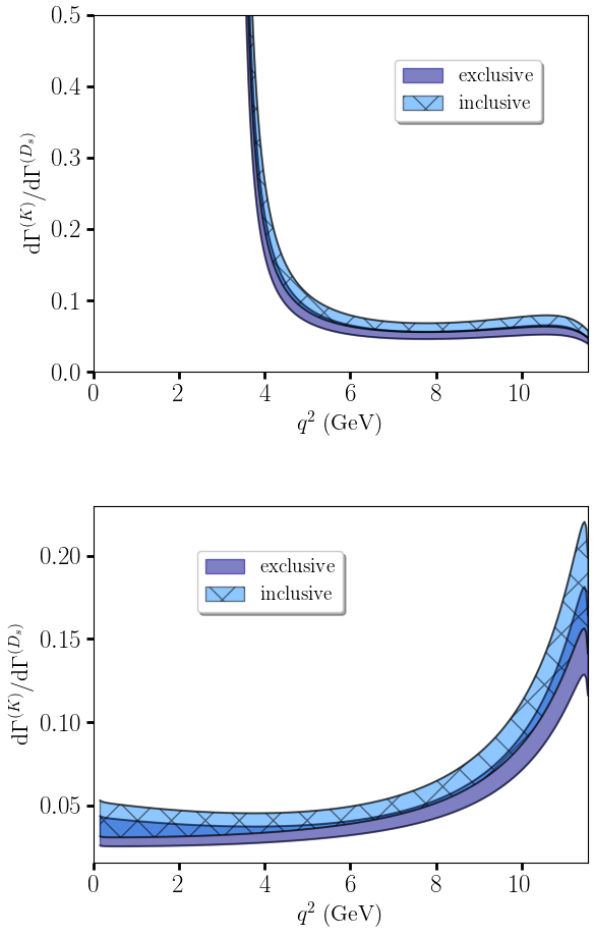

Defining the partially integrated ratio

$$\zeta_\ell^{(X_s)} = \frac{1}{|V_{xb}|^2}\int_{m_\ell^2}^{q^2_{\rm max}} \frac{{\rm d}\Gamma(B_s \to X_s \ell\nu)}{{\rm d}q^2}{\rm d}q^2, \tag{31}$$

where $q^2_{\rm max} = (M_{B_s} - M_{X_s})^2$, we integrate our results numerically to obtain

$$\frac{\zeta_\mu^{(K)}}{\zeta_\mu^{(D_s)}} = 0.85(13), \tag{32}$$

$$\frac{\zeta_\tau^{(K)}}{\zeta_\tau^{(D_s)}} = 1.72(19). \tag{33}$$

Asymmetries in the differential decay rate can be defined from the angular distribution, Eq. (27). The forward-backward asymmetry is given by

$$\begin{aligned} A_\ell^{(X_s)}(q^2) &= \left[\int_0^1 - \int_{-1}^0\right] {\rm d}\cos\theta_\ell \frac{{\rm d}^2\Gamma}{{\rm d}q^2 {\rm d}\cos\theta_\ell} \\ &= \frac{G_F^2|V_{xb}|^2}{32\pi^3 M_{B_s}}\left(1-\frac{m_\ell^2}{q^2}\right)^2 |\vec{p}_{X_s}|^2 \frac{m_\ell^2}{q^2} \\ &\quad \times \left(M_{B_s}^2 - M_{X_s}^2\right) f_0 f_+, \end{aligned} \tag{34}$$

and the polarization asymmetry by

$$P_\ell^{(X_s)}(q^2) = \frac{{\rm d}\Gamma({\rm LH})}{{\rm d}q^2} - \frac{{\rm d}\Gamma({\rm RH})}{{\rm d}q^2}, \tag{35}$$

where the differential decay rates to left-handed (LH) and right-handed (RH) final state leptons are given by

$$\frac{{\rm d}\Gamma({\rm LH})}{{\rm d}q^2} = \frac{G_F^2|V_{xb}|^2|\vec{p}_{X_s}|^3}{24\pi^3}\left(1-\frac{m_\ell^2}{q^2}\right)^2 f_+^2, \tag{36}$$

$$\begin{aligned} \frac{{\rm d}\Gamma({\rm RH})}{{\rm d}q^2} &= \frac{G_F^2|V_{xb}|^2|\vec{p}_{X_s}|^3}{24\pi^3}\frac{m_\ell^2}{q^2}\left(1-\frac{m_\ell^2}{q^2}\right)^2 \\ &\quad \times \left[\frac{3}{8}\frac{(M_{B_s}^2 - M_{X_s}^2)^2}{M_{B_s}^2} f_0^2 + \frac{1}{2}|\vec{p}_{X_s}|^2 f_+^2\right]. \end{aligned} \tag{37}$$

In the standard model, the production of right-handed final state leptons is helicity suppressed, and so this asymmetry offers a probe for helicity-violating interactions generated by new physics.

In Figs. 8 and 9, we plot the ratios of the forward-backward and polarization asymmetries, respectively, for the $B_s \to K\ell\nu$ and $B_s \to D_s\ell\nu$ decays. We plot the asymmetry ratios using both inclusive and exclusive values of $|V_{ub}/V_{cb}|$. Integrating over q^2, and multiplying by the appropriate combination of CKM matrix elements to define the QCD contribution, we find

$$\frac{|V_{cb}|^2}{|V_{ub}|^2}\frac{\int_{m_\ell^2}^{q^2_{\rm max}} A_\mu^{(K)}{\rm d}q^2}{\int_{m_\mu^2}^{q^2_{\rm max}} A_\mu^{(D_s)}{\rm d}q^2} = 0.399(85), \tag{38}$$

$$\frac{|V_{cb}|^2}{|V_{ub}|^2}\frac{\int_{m_\ell^2}^{q^2_{\rm max}} A_\tau^{(K)}{\rm d}q^2}{\int_{m_\tau^2}^{q^2_{\rm max}} A_\tau^{(D_s)}{\rm d}q^2} = 1.38(15), \tag{39}$$

$$\frac{|V_{cb}|^2}{|V_{ub}|^2}\frac{\int_{m_\ell^2}^{q^2_{\rm max}} P_\mu^{(K)}{\rm d}q^2}{\int_{m_\mu^2}^{q^2_{\rm max}} P_\mu^{(D_s)}{\rm d}q^2} = 0.87(13), \tag{40}$$

$$\frac{|V_{cb}|^2}{|V_{ub}|^2}\frac{\int_{m_\ell^2}^{q^2_{\rm max}} P_\tau^{(K)}{\rm d}q^2}{\int_{m_\tau^2}^{q^2_{\rm max}} P_\tau^{(D_s)}{\rm d}q^2} = -0.42(22). \tag{41}$$

Normalizing these asymmetry ratios by the corresponding differential decay rate ratio removes the am-

FIG. 8. Ratio of the forward-backward asymmetries, $A_\tau^{(K)}/A_\tau^{(D_s)}$ (upper panel) and $A_\mu^{(K)}/A_\mu^{(D_s)}$ (lower panel), using inclusive and exclusive world average results for $|V_{ub}/V_{cb}|$, as a function of the momentum transfer, q^2.

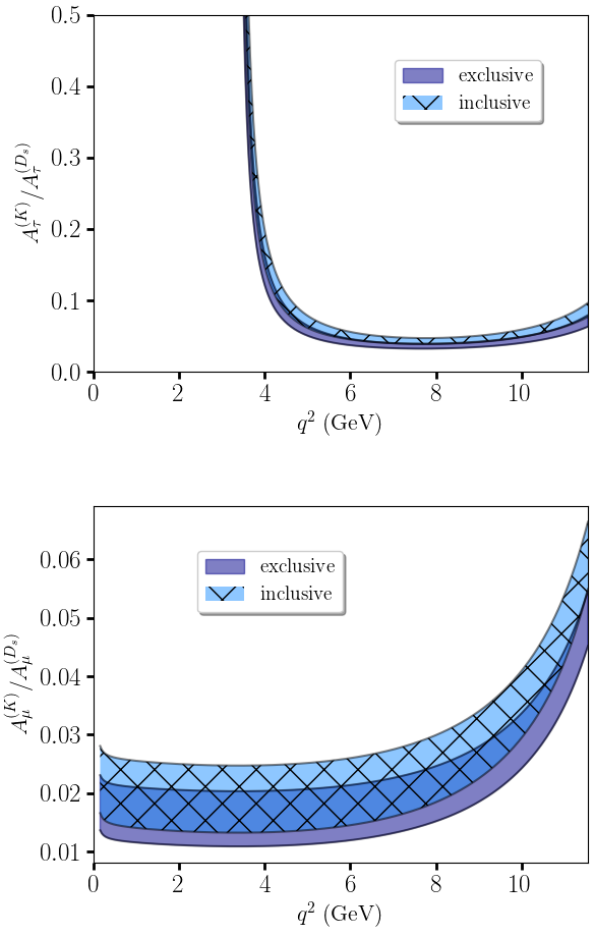

FIG. 9. Ratio of the polarization asymmetries, $P_\tau^{(K)}/P_\tau^{(D_s)}$ (upper panel) and $P_\mu^{(K)}/P_\mu^{(D_s)}$ (lower panel), using inclusive and exclusive world average results for $|V_{ub}/V_{cb}|$, as a function of the momentum transfer, q^2.

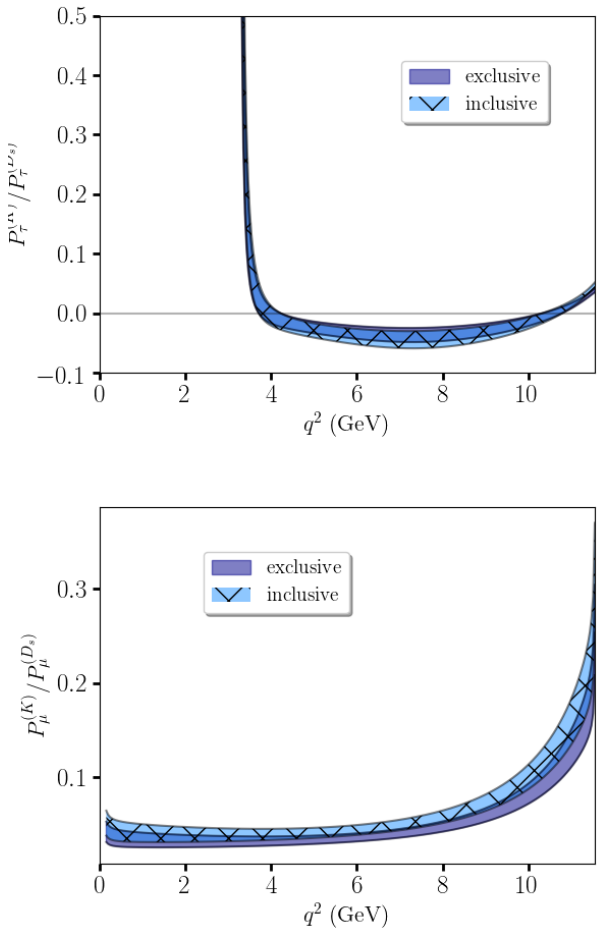

biguity arising from $|V_{ub}/V_{cb}|$,

$$\overline{A}_\ell^{(X_s)} = \frac{\int_{m_\ell^2}^{q^2_{\rm max}} A_\ell^{(X_s)} {\rm d}q^2}{\int_{m_\ell^2}^{q^2_{\rm max}} ({\rm d}\Gamma/{\rm d}q^2){\rm d}q^2}, \tag{42}$$

$$\overline{P}_\ell^{(X_s)} = \frac{\int_{m_\ell^2}^{q^2_{\rm max}} P_\ell^{(X_s)} {\rm d}q^2}{\int_{m_\ell^2}^{q^2_{\rm max}} ({\rm d}\Gamma/{\rm d}q^2){\rm d}q^2}. \tag{43}$$

We integrate over the momentum transfer numerically to find

$$\frac{\overline{A}_\mu^{(K)}}{\overline{A}_\mu^{(D_s)}} = 0.470(41), \qquad \frac{\overline{P}_\mu^{(K)}}{\overline{P}_\mu^{(D_s)}} = 1.0193(17) \tag{44}$$

$$\frac{\overline{A}_\tau^{(K)}}{\overline{A}_\tau^{(D_s)}} = 0.804(15), \qquad \frac{\overline{P}_\tau^{(K)}}{\overline{P}_\tau^{(D_s)}} = -0.25(11), \tag{45}$$

where the smaller relative uncertainties compared to the asymmetries themselves demonstrates that most of the hadronic uncertainties have canceled in these normalized results.

VI. SUMMARY

We have presented a study of the ratio of the scalar and vector form factors for the $B_s \to X_s \ell\nu$ semileptonic decays, where X_s is a K or D_s meson, over the full kinematic range of momentum transfer. These ratios combine correlator data results determined in [46] for the $B_s \to K$ decay and in [47] for the $B_s \to D_s$ decay. Our simultaneous, correlated chiral-continuum kinematic extrapolation reduces the uncertainty in the form factor ratio and, in particular, largely removes the uncertainty arising from the perturbative matching procedure.

In addition to the form factor ratios, we predict $R(K)/R(D_s)$, where $R(X_s)$ is the ratio of the branching fractions of the corresponding semileptonic B_s decay to

TABLE VII. Fit results for the ground state energies of the K meson at each spatial momentum $\vec{p}_K$. Data reproduced from Table V of [46].

Set	aM_K	$aE_K(1,0,0)$	$aE_K(1,1,0)$	$aE_K(1,1,1)$
C1	0.31211(15)	0.40657(58)	0.48461(76)	0.5511(16)
C2	0.32863(18)	0.54506(85)	0.5511(16)	0.6261(75)
C3	0.35717(22)	0.47521(85)	0.5723(11)	0.6524(30)
F1	0.22865(11)	0.32024(66)	0.39229(86)	0.4515(25)
F2	0.24577(13)	0.33322(52)	0.40214(73)	0.4623(14)

TABLE VIII. Fit results for the ground state energies of the D_s meson at each spatial momentum $\vec{p}_{D_s}$. Data reproduced from Table IV of [47].

Set	aM_{D_s}	$aE_{D_s}(1,0,0)$	$aE_{D_s}(1,1,0)$	$aE_{D_s}(1,1,1)$
C1	1.18755(22)	1.21517(34)	1.24284(33)	1.27013(39)
C2	1.20090(30)	1.24013(56)	1.27822(61)	1.31543(97)
C3	1.19010(33)	1.23026(53)	1.26948(54)	1.30755(79)
F1	0.84674(12)	0.87559(19)	0.90373(20)	0.93096(26)
F2	0.84415(14)	0.87348(25)	0.90145(25)	0.92869(33)

tau and to electrons and muons. We determine the ratio of the differential decay rates for the two decay channels, as well as the ratio of the forward-backward and polarization asymmetries.

The LHC is scheduled to significantly improve the statistical uncertainties in experimental measurements of B_s decays with more data over the next decade. In particular, experimental data on the ratio of the $B_s \to K\ell\nu$ and $B_s \to D_s\ell\nu$ decays, when combined with our form factor results, will provide a new determination of $|V_{ub}/V_{cb}|$.

ACKNOWLEDGMENTS

Numerical simulations were carried out on facilities of the USQCD Collaboration funded by the Office of Science of the Department of Energy and at the Ohio Supercomputer Center. Parts of this work were supported by the National Science Foundation. C.J.M. was supported in part by the U.S. Department of Energy through Grant No. DE-FG02-00ER41132 and J.S. in part by the U.S. Department of Energy through Grant No. desc0011726. We thank the MILC Collaboration for use of their gauge configurations.

Appendix A: Two-point fit results

Here we reproduce the two-point fit results of [46] in Table VII for the K meson and for the D_s meson [47] in Table VIII.

Appendix B: Reconstructing form factors

In this Appendix we provide our fit results for the coefficients of the z-expansion for the $B_s \to K\ell\nu$ decay in Table IX, for $B_s \to D_s\ell\nu$ in Table X, and for the correlated fit to both decays in Table XI. We also tabulate our choice of priors for the chiral-continuum extrapolation for the $B_s \to K\ell\nu$ decay in Tables XII and XIV, for the $B_s \to D_s\ell\nu$ decay in Tables XIII and XV, and for priors common to both channels in XVI, and XVII.

TABLE IX. Coefficients of z-expansion and the corresponding Blaschke factors for the $B_s \to K\ell\nu$ decay.

$a_1^{(0)}$	$a_2^{(0)}$	$a_3^{(0)}$	P_0	$a_0^{(+)}$	$a_1^{(+)}$	$a_2^{(+)}$	P_+
0.336(88)	1.23(70)	2.1(2.6)	5.6793(10)	0.301(18)	-0.48(12)	2.39(86)	5.32450(27)

TABLE X. Coefficients of z-expansion and the corresponding Blaschke factors, for the $B_s \to D_s\ell\nu$ decay.

$a_0^{(0)}$	$a_1^{(0)}$	$a_2^{(0)}$	$a_3^{(0)}$	P_0	$a_0^{(+)}$	$a_1^{(+)}$	$a_2^{(+)}$	P_+
0.673(39)	-0.02(34)	1.4(2.8)	-0.1(3.0)	6.41(10)	0.773(37)	-3.01(56)	-0.01(2.95)	6.3300(90)

TABLE XI. Covariance matrix for the coefficients of z-expansion and the corresponding Blaschke factors for the simultaneous fit to the $B_s \to K\ell\nu$ and $B_s \to D_s\ell\nu$ decays. The rows correspond to the columns, moving from top to bottom and left to right, respectively.

$a_1^{(0),K}$	$a_2^{(0),K}$	$a_3^{(0),K}$	$P_0^{(K)}$	$a_0^{(+),K}$	$a_1^{(+),K}$
7.81655746×10^{-3}	5.11931999×10^{-2}	1.26040746×10^{-1}	-3.95599616×10^{-7}	6.67729571×10^{-4}	7.88936302×10^{-3}
	4.94505240×10^{-1}	1.62865239	2.22974369×10^{-6}	3.58512534×10^{-3}	6.75709862×10^{-2}
		6.51816994	-4.88348307×10^{-8}	9.03252850×10^{-3}	1.99167048×10^{-1}
			9.99995307×10^{-7}	-1.81816269×10^{-9}	1.55891061×10^{-7}
				3.09228616×10^{-4}	-5.88646696×10^{-5}
					1.46893824×10^{-2}

$a_2^{(+),K}$	$P_+^{(K)}$	$a_0^{(0),D_s}$	$a_1^{(0),D_s}$	$a_2^{(0),D_s}$	$a_3^{(0),D_s}$
5.54055868×10^{-2}	5.22263419×10^{-9}	4.89761879×10^{-5}	1.47978430×10^{-3}	1.61294090×10^{-4}	-1.50864482×10^{-5}
5.20212224×10^{-1}	4.60220124×10^{-8}	4.23550639×10^{-4}	-1.12557927×10^{-3}	-4.15916006×10^{-4}	6.86722615×10^{-6}
1.72576055	1.64613013×10^{-7}	5.32746249×10^{-4}	-8.00096682×10^{-3}	-1.57760368×10^{-3}	6.07028861×10^{-5}
1.27709131×10^{-6}	4.34812507×10^{-15}	-2.93868039×10^{-9}	3.60812633×10^{-8}	3.12552274×10^{-9}	$-2.93053824\times10^{-10}$
5.57789886×10^{-4}	3.44350904×10^{-9}	1.08803466×10^{-4}	7.14515361×10^{-4}	1.46191770×10^{-4}	-9.57576314×10^{-6}
6.49789179×10^{-2}	-1.42002142×10^{-7}	2.37456520×10^{-4}	-7.74705909×10^{-3}	-1.63296714×10^{-3}	9.27876845×10^{-5}
7.40157233×10^{-1}	8.20182628×10^{-7}	9.33127619×10^{-4}	3.38332719×10^{-4}	-1.12948406×10^{-5}	-1.17310027×10^{-5}
	5.28997606×10^{-8}	$-4.00252884\times10^{-11}$	1.55683903×10^{-10}	8.25859041×10^{-11}	4.62131689×10^{-12}
		1.51331616×10^{-3}	-1.32946477×10^{-3}	-2.95921529×10^{-3}	-1.18940865×10^{-4}
			1.14391084×10^{-1}	3.77594136×10^{-1}	-1.47064962×10^{-2}
				8.04802477	6.00685427×10^{-2}
					8.99580234

$P_0^{(D_s)}$	$a_0^{(+),D_s}$	$a_1^{(+),D_s}$	$a_2^{(+),D_s}$	$P_+^{(D_s)}$
2.48190307×10^{-6}	1.25952168×10^{-4}	-1.00202940×10^{-3}	3.13648146×10^{-5}	-1.42966100×10^{-8}
1.66495291×10^{-6}	4.16420952×10^{-4}	-8.93653944×10^{-4}	4.32425257×10^{-4}	-3.15809640×10^{-8}
-3.14364934×10^{-6}	2.30951064×10^{-4}	1.62406281×10^{-3}	1.00576304×10^{-3}	8.26930192×10^{-10}
5.51018709×10^{-11}	-1.49607346×10^{-9}	-1.05105378×10^{-8}	3.28268609×10^{-10}	$-4.41710197\times10^{-14}$
7.04107924×10^{-7}	1.61718771×10^{-4}	-9.47821843×10^{-4}	-7.78344712×10^{-6}	-1.33434640×10^{-8}
-6.39749633×10^{-6}	-1.59677031×10^{-4}	4.95080220×10^{-3}	5.36015327×10^{-4}	2.94137887×10^{-8}
2.60283535×10^{-6}	1.06965630×10^{-3}	-3.87458330×10^{-3}	3.61587037×10^{-4}	-8.16004467×10^{-8}
$-1.19874155\times10^{-12}$	$-3.95882072\times10^{-11}$	2.69588869×10^{-10}	$-1.34953976\times10^{-10}$	2.49776863×10^{-15}
3.86973615×10^{-4}	1.25442551×10^{-3}	7.19766977×10^{-3}	7.34363847×10^{-3}	-6.23834522×10^{-7}
-1.51873367×10^{-2}	1.80319837×10^{-3}	2.26955835×10^{-2}	2.65518223×10^{-2}	-2.61624148×10^{-6}
4.53224736×10^{-3}	1.19829415×10^{-2}	1.18533968×10^{-1}	2.29348564×10^{-1}	-2.65313186×10^{-5}
-2.72916676×10^{-4}	-1.76329307×10^{-4}	-1.96104068×10^{-3}	-8.21918389×10^{-3}	1.15675448×10^{-6}
9.95331216×10^{-3}	-5.12869129×10^{-5}	-5.75838181×10^{-4}	-9.37738726×10^{-4}	1.10417128×10^{-7}
	1.37380763×10^{-3}	-1.31877655×10^{-3}	-8.10703811×10^{-3}	4.47444315×10^{-6}
		3.21831236×10^{-1}	2.71750438×10^{-1}	-1.70915346×10^{-4}
			8.72142922	4.09895485×10^{-5}
				8.10107530×10^{-5}

TABLE XII. Group I priors and fit results for the parameters in the modified z-expansion for the $B_s \to K\ell\nu$ decay. Note that these parameters are fit simultaneously with those of Table XIII, but displayed separately for clarity.

	Prior $[f_0]$	Fit result $[f_0]$	Prior $[f_+]$	Fit result $[f_+]$
a_1	0.0(3.0)	0.336(88)	0.0(5.0)	0.301(43)
a_2	0.0(3.0)	1.23(70)	0.0(5.0)	-0.48(23)
a_3	0.0(3.0)	2.1(2.6)	0.0(5.0)	2.39(86)
$c_1^{(1)}$	0.0(1.0)	-0.17(48)	0.0(1.0)	0.222(89)
$c_2^{(1)}$	0.0(1.0)	0.34(72)	0.0(1.0)	0.52(48)
$c_3^{(1)}$	0.0(1.0)	0.002(976)	0.0(1.0)	-0.11(65)
$d_1^{(1)}$	0.00(30)	-0.08(30)	0.00(30)	0.03(26)
$d_2^{(1)}$	0.00(30)	0.02(30)	0.00(30)	0.02(30)
$d_3^{(1)}$	0.00(30)	0.002(300)	0.00(30)	0.02(30)
$d_1^{(2)}$	0.0(1.0)	0.3(1.0)	0.00(30)	0.04(97)
$d_2^{(2)}$	0.0(1.0)	-0.2(1.0)	0.00(30)	0.007(1.0)
$d_3^{(2)}$	0.0(1.0)	0.04(1.0)	0.00(30)	0.004(1.0)
$e_1^{(1)}$	0.00(30)	0.0007(0.3)	0.00(30)	0.013(28)
$e_2^{(1)}$	0.00(30)	0.006(0.3)	0.00(30)	0.0007(0.3)
$e_3^{(1)}$	0.00(30)	-0.002(0.3)	0.00(30)	-0.003(0.3)
$e_1^{(2)}$	0.0(1.0)	0.006(1.0)	0.0(1.0)	0.01(30)
$e_2^{(2)}$	0.0(1.0)	-0.001(1.0)	0.0(1.0)	0.0005(1.0)
$e_3^{(2)}$	0.0(1.0)	-0.0001(1.0)	0.0(1.0)	3×10^{-5}(1.0)
$f_1^{(1)}$	0.00(30)	-0.20(27)	0.00(30)	0.24(19)
$f_2^{(1)}$	0.00(30)	0.14(29)	0.00(30)	-0.08(29)
$f_3^{(1)}$	0.00(30)	-0.03(30)	0.00(30)	-0.03(30)
$f_1^{(2)}$	0.0(1.0)	-0.47(94)	0.0(1.0)	0.28(83)
$f_2^{(2)}$	0.0(1.0)	0.33(98)	0.0(1.0)	-0.13(99)
$f_3^{(2)}$	0.0(1.0)	-0.08(1.0)	0.0(1.0)	-0.08(1.0)
$l_1^{(1,1)}$	0.0(1.0)	-0.21(98)	0.0(1.0)	0.09(99)
$l_2^{(1,1)}$	0.0(1.0)	-0.06(1.0)	0.0(1.0)	0.03(1.0)
$l_3^{(1,1)}$	0.0(1.0)	-0.0005(1.0)	0.0(1.0)	0.002(1.0)
$l_1^{(1,2)}$	0.0(1.0)	-0.07(1.0)	0.0(1.0)	0.06(1.0)
$l_2^{(1,2)}$	0.0(1.0)	-0.02(1.0)	0.0(1.0)	0.002(1.0)
$l_3^{(1,2)}$	0.0(1.0)	-0.0006(1.0)	0.0(1.0)	-0.0003(1.0)
$l_1^{(2,1)}$	0.0(1.0)	-0.06(1.0)	0.0(1.0)	-0.02(1.0)
$l_2^{(2,1)}$	0.0(1.0)	-0.003(1.0)	0.0(1.0)	0.009(1.0)
$l_3^{(2,1)}$	0.0(1.0)	0.0007(1.0)	0.0(1.0)	0.003(1.0)
$l_1^{(2,2)}$	0.0(1.0)	-0.03(1.0)	0.0(1.0)	-0.0003(1.0)
$l_2^{(2,2)}$	0.0(1.0)	-0.007(1.0)	0.0(1.0)	0.001(1.0)
$l_3^{(2,2)}$	0.0(1.0)	-0.0002(1.0)	0.0(1.0)	0.0004(1.0)
$h_1^{(1,1)}$	0.0(1.0)	-0.21(98)	0.0(1.0)	-0.49(61)
$h_2^{(1,1)}$	0.0(1.0)	-0.06(1.0)	0.0(1.0)	0.2(1.0)
$h_3^{(1,1)}$	0.0(1.0)	-0.0005(1.0)	0.0(1.0)	0.03(1.0)
$h_1^{(1,2)}$	0.0(1.0)	-0.07(1.0)	0.0(1.0)	-0.04(97)
$h_2^{(1,2)}$	0.0(1.0)	-0.02(1.0)	0.0(1.0)	0.03(1.0)
$h_3^{(1,2)}$	0.0(1.0)	-0.0006(1.0)	0.0(1.0)	0.004(1.0)
$h_1^{(2,1)}$	0.0(1.0)	-0.06(1.0)	0.0(1.0)	-0.11(1.0)
$h_2^{(2,1)}$	0.0(1.0)	-0.003(1.0)	0.0(1.0)	0.03(1.0)
$h_3^{(2,1)}$	0.0(1.0)	0.0007(1.0)	0.0(1.0)	0.01(1.0)
$h_1^{(2,2)}$	0.0(1.0)	-0.03(1.0)	0.0(1.0)	-0.04(1.0)
$h_2^{(2,2)}$	0.0(1.0)	-0.007(1.0)	0.0(1.0)	0.01(1.0)
$h_3^{(2,2)}$	0.0(1.0)	-0.0002(1.0)	0.0(1.0)	0.003(1.0)

TABLE XIII. Group I priors and fit results for the parameters in the modified z-expansion for the $B_s \to D_s\ell\nu$ decay. Note that these parameters are fit simultaneously with those of Table XII, but displayed separately for clarity.

	Prior $[f_0]$	Fit result $[f_0]$	Prior $[f_+]$	Fit result $[f_+]$
a_0	0.0(3.0)	0.673(39)	0.0(5.0)	0.773(37)
a_1	0.0(3.0)	-0.02(34)	0.0(5.0)	-3.01(56)
a_2	0.0(3.0)	1.4(2.8)	0.0(5.0)	-0.01(2.95)
a_3	0.0(3.0)	-0.1(3.0)	-	-
$c_0^{(1)}$	0.0(1.0)	0.087(15)	0.0(1.0)	0.188(69)
$c_1^{(1)}$	0.0(1.0)	-0.03(1.0)	0.0(1.0)	0.61(46)
$c_2^{(1)}$	0.0(1.0)	-0.09(1.0)	0.0(1.0)	-0.0001(1.0)
$c_3^{(1)}$	0.0(1.0)	-0.0002(1.0)	-	-
$c_0^{(2)}$	0.00(30)	0.006(31)	0.00(30)	0.165(67)
$c_1^{(2)}$	0.00(30)	0.003(300)	0.00(30)	0.06(29)
$c_2^{(2)}$	0.00(30)	0.005(30)	0.00(30)	-7×10^{-6}(0.3)
$c_3^{(2)}$	0.00(30)	5×10^{-6}(0.3)	-	-
$d_0^{(1)}$	0.00(30)	-0.36(16)	0.00(30)	-0.52(17)
$d_1^{(1)}$	0.00(30)	-0.0006(0.3)	0.00(30)	-0.03(30)
$d_2^{(1)}$	0.00(30)	-0.0002(0.3)	0.00(30)	2×10^{-6}(0.3)
$d_3^{(2)}$	0.00(30)	3×10^{-6}(0.3)	-	-
$d_0^{(2)}$	0.00(30)	0.06(30)	0.00(30)	0.11(30)
$d_1^{(2)}$	0.00(30)	7×10^{-5}(0.3)	0.00(30)	0.01(30)
$d_2^{(2)}$	0.00(30)	1×10^{-4}(0.3)	0.00(30)	-1×10^{-6}(0.3)
$d_2^{(3)}$	0.00(30)	2×10^{-7}(0.3)	-	-
$e_0^{(1)}$	0.00(30)	0.17(25)	0.00(30)	0.18(23)
$e_1^{(1)}$	0.00(30)	-0.0008(0.3)	0.00(30)	-0.02(30)
$e_2^{(1)}$	0.00(30)	0.0008(0.3)	0.00(30)	5×10^{-6}(0.3)
$e_3^{(1)}$	0.00(30)	1×10^{-5}(0.3)	-	-
$e_0^{(2)}$	0.0(1.0)	1.51(53)	0.0(1.0)	0.06(29)
$e_1^{(2)}$	0.0(1.0)	-0.002(1.0)	0.0(1.0)	-0.001(1.0)
$e_2^{(2)}$	0.0(1.0)	-0.002(1.0)	0.0(1.0)	1×10^{-6}(1.0)
$e_3^{(2)}$	0.0(1.0)	9×10^{-6}(1.0)	-	-
$m_0^{(1)}$	0.00(30)	-0.004(0.229)	0.00(30)	0.15(23)
$m_1^{(1)}$	0.00(30)	-0.0003(0.3)	0.00(30)	-0.09(28)
$m_2^{(1)}$	0.00(30)	0.008(0.3)	0.00(30)	2×10^{-5}(0.3)
$m_3^{(1)}$	0.00(30)	4×10^{-5}(0.3)	-	-
$m_0^{(2)}$	0.0(1.0)	-0.49(40)	0.0(1.0)	-0.34(42)
$m_1^{(2)}$	0.0(1.0)	-0.003(1.0)	0.0(1.0)	-0.74(81)
$m_2^{(2)}$	0.0(1.0)	0.03(1.0)	0.0(1.0)	0.0001(1.0)
$m_3^{(2)}$	0.0(1.0)	0.0002(1.0)	-	-

TABLE XIV. Group II priors and fit results for the parameters in the modified z-expansion for the $B_s \to K\ell\nu$ decay.

Quantity	Prior	Fit result
$aE_K(0,0,0)$	0.31195(14)	0.31197(14)
	0.32870(17)	0.32865(17)
	0.35744(21)	0.35747(21)
	0.22861(12)	0.22862(12)
	0.24566(13)	0.24565(13)
$aE_K(1,0,0)$	0.40661(49)	0.40662(48)
	0.45434(73)	0.45432(70)
	0.47507(71)	0.47566(69)
	0.32020(61)	0.31986(58)
	0.33310(50)	0.33293(49)
$aE_K(1,1,0)$	0.48408(63)	0.48393(62)
	0.5506(11)	0.5511(11)
	0.57218(80)	0.57168(78)
	0.39192(82)	0.39240(79)
	0.40184(72)	0.40204(70)
$aE_K(1,1,1)$	0.5513(13)	0.5511(13)
	0.6273(35)	0.6290(34)
	0.6539(18)	0.6534(17)
	0.4528(16)	0.4527(15)
	0.4624(11)	0.4624(11)
M_+	5.32450(27)	5.32450(27)
M_0	5.6793(10)	5.6793(10)

TABLE XV. Group II priors and fit results for the parameters in the modified z-expansion for the $B_s \to D_s\ell\nu$ decay.

Quantity	Prior	Fit result
$aE_{D_s}(0,0,0)$	1.18750(15)	1.18749(15)
	1.20126(21)	1.20132(20)
	1.19031(24)	1.19020(24)
	0.84674(12)	0.84674(12)
	0.84419(10)	0.84421(10)
$aE_{D_s}(1,0,0)$	1.21497(19)	1.21504(19)
	1.24055(30)	1.24080(28)
	1.23055(35)	1.23055(31)
	0.87575(18)	0.87574(18)
	0.87353(16)	0.87345(15)
$aE_{D_s}(1,1,0)$	1.24264(19)	1.24274(19)
	1.27942(29)	1.27958(26)
	1.26974(35)	1.26941(32)
	0.90393(18)	0.90392(18)
	0.90144(16)	0.90148(15)
$aE_{D_s}(1,1,1)$	1.26988(22)	1.26997(22)
	1.31755(46)	1.31737(39)
	1.30768(48)	1.30727(41)
	0.93126(24)	0.93123(24)
	0.92873(20)	0.92880(20)
M_+	6.3300(90)	6.3300(90)
M_0	6.41(10)	6.41(10)

TABLE XVI. Group II priors and fit results for the parameters in the modified z-expansion, common to both $B_s \to X_s\ell\nu$ decay channels.

Quantity	Prior	Fit result
r_1/a	2.6470(30)	2.6463(28)
	2.6180(30)	2.6209(27)
	2.6440(30)	2.6423(29)
	3.6990(30)	3.6984(30)
	3.7120(40)	3.7127(40)
aM_B	3.18915(65)	3.18921(64)
	3.23184(88)	3.23136(85)
	3.21191(77)	3.21221(76)
	2.28109(52)	2.28120(51)
	2.28101(44)	2.28093(44)
aM_{B_s}	3.23019(25)	3.23012(25)
	3.26785(33)	3.26792(33)
	3.23585(38)	3.23566(38)
	2.30906(26)	2.30899(25)
	2.30122(16)	2.30124(16)
aM_π	0.15990(20)	0.15990(20)
	0.21110(20)	0.21110(20)
	0.29310(20)	0.29310(20)
	0.13460(10)	0.13460(10)
	0.18730(10)	0.18730(10)
aM_{η_s}	0.41113(18)	0.41113(18)
	0.41435(22)	0.41433(22)
	0.41185(22)	0.41186(22)
	0.29416(12)	0.29416(12)
	0.29311(18)	0.29311(18)
$aM_\pi^{\rm MILC}$	0.15971(20)	0.15971(20)
	0.22447(17)	0.22448(17)
	0.31125(16)	0.31124(16)
	0.14789(18)	0.14789(18)
	0.20635(18)	0.20636(18)
$aM_K^{\rm MILC}$	0.36530(29)	0.36526(29)
	0.38331(24)	0.38337(24)
	0.40984(21)	0.40981(21)
	0.25318(19)	0.25317(19)
	0.27217(21)	0.27219(21)
$1+m_\parallel$	1.000(40)	1.001(40)
$1+m_\perp$	1.000(40)	1.000(40)

TABLE XVII. Group III priors and fit results for the parameters in the modified z-expansion, common to both $B_s \to K\ell\nu$ and $B_s \to D_s\ell\nu$ decays.

Quantity	Prior (GeV)	Fit result (GeV)
r_1	0.3129(23)	0.3130(23)
$M_\pi^{\rm phys}$	0.13497700(50)	0.13497700(50)
$M_K^{\rm phys}$	0.495644(26)	0.495644(26)
$M_\eta^{\rm phys}$	0.547862(17)	0.547862(17)
$M_{\eta_s}^{\rm phys}$	0.6858(40)	0.6857(40)
$M_{D_s}^{\rm phys}$	1.96828(10)	1.96828(10)
$M_{B_s}^{\rm phys}$	5.36689(23)	5.36689(23)

[1] M. Tanabashi et al. (Particle Data Group), Phys. Rev. D **98**, 030001 (2018).
[2] Y. Amhis et al. (HFLAV), Eur. Phys. J. **C77**, 895 (2017), 1612.07233.
[3] B. Aubert et al. (BaBar), Phys. Rev. Lett. **97**, 211801 (2006), hep-ex/0607089.
[4] T. Hokuue et al. (Belle), Phys. Lett. **B648**, 139 (2007), hep-ex/0604024.
[5] N. E. Adam et al. (CLEO), Phys. Rev. Lett. **99**, 041802 (2007), hep-ex/0703041.
[6] R. Gray et al. (CLEO), Phys. Rev. **D76**, 012007 (2007), [Addendum: Phys. Rev.D76,no.3,039901(2007)], hep-ex/0703042.
[7] B. Aubert et al. (BaBar), Phys. Rev. Lett. **101**, 081801 (2008), 0805.2408.
[8] P. del Amo Sanchez et al. (BaBar), Phys. Rev. **D83**, 032007 (2011), 1005.3288.
[9] P. del Amo Sanchez et al. (BaBar), Phys. Rev. **D83**, 052011 (2011), 1010.0987.
[10] H. Ha et al. (Belle), Phys. Rev. **D83**, 071101 (2011), 1012.0090.
[11] A. Sibidanov et al. (Belle), Phys. Rev. **D88**, 032005 (2013), 1306.2781.
[12] D. Buskulic et al. (ALEPH), Phys. Lett. **B395**, 373 (1997).
[13] G. Abbiendi et al. (OPAL), Phys. Lett. **B482**, 15 (2000), hep-ex/0003013.
[14] P. Abreu et al. (DELPHI), Phys. Lett. **B510**, 55 (2001), hep-ex/0104026.
[15] J. Abdallah et al. (DELPHI), Eur. Phys. J. **C33**, 213 (2004), hep-ex/0401023.
[16] N. E. Adam et al. (CLEO), Phys. Rev. **D67**, 032001 (2003), hep-ex/0210040.
[17] B. Aubert et al. (BaBar), Phys. Rev. **D77**, 032002 (2008), 0705.4008.
[18] B. Aubert et al. (BaBar), Phys. Rev. Lett. **100**, 231803 (2008), 0712.3493.
[19] B. Aubert et al. (BaBar), Phys. Rev. **D79**, 012002 (2009), 0809.0828.
[20] W. Dungel et al. (Belle), Phys. Rev. **D82**, 112007 (2010), 1010.5620.
[21] B. Aubert et al. (BaBar), Phys. Rev. Lett. **90**, 181801 (2003), [eConfC0304052,WG117(2003)], hep-ex/0301001.
[22] C. Schwanda et al. (Belle), Phys. Rev. Lett. **93**, 131803 (2004), hep-ex/0402023.
[23] B. Aubert et al. (BaBar), Phys. Rev. **D79**, 052011 (2009), 0808.3524.
[24] J. P. Lees et al. (BaBar), Phys. Rev. **D87**, 032004 (2013), [Erratum: Phys. Rev.D87,no.9,099904(2013)], 1205.6245.
[25] J. P. Lees et al. (BaBar), Phys. Rev. **D88**, 072006 (2013), 1308.2589.
[26] E. Dalgic, A. Gray, M. Wingate, C. T. H. Davies, G. P. Lepage, and J. Shigemitsu, Phys. Rev. **D73**, 074502 (2006), [Erratum: Phys. Rev.D75,119906(2007)], hep-lat/0601021.
[27] B. Colquhoun, R. J. Dowdall, J. Koponen, C. T. H. Davies, and G. P. Lepage, Phys. Rev. **D93**, 034502 (2016), 1510.07446.
[28] J. A. Bailey et al. (Fermilab Lattice, MILC), Phys. Rev. **D92**, 014024 (2015), 1503.07839.
[29] J. M. Flynn, T. Izubuchi, T. Kawanai, C. Lehner, A. Soni, R. S. Van de Water, and O. Witzel, Phys. Rev. **D91**, 074510 (2015), 1501.05373.
[30] J. A. Bailey et al. (Fermilab Lattice, MILC), Phys. Rev. **D89**, 114504 (2014), 1403.0635.
[31] H. Na, C. M. Bouchard, G. P. Lepage, C. Monahan, and J. Shigemitsu (HPQCD), Phys. Rev. **D92**, 054510 (2015), [Erratum: Phys. Rev.D93,no.11,119906(2016)], 1505.03925.
[32] J. A. Bailey et al. (MILC), Phys. Rev. **D92**, 034506 (2015), 1503.07237.
[33] J. Harrison, C. Davies, and M. Wingate (HPQCD), Phys. Rev. **D97**, 054502 (2018), 1711.11013.
[34] P. Ball and R. Zwicky, Phys. Rev. **D71**, 014015 (2005), hep-ph/0406232.
[35] G. Duplancic, A. Khodjamirian, T. Mannel, B. Melic, and N. Offen, JHEP **04**, 014 (2008), 0801.1796.
[36] A. Khodjamirian, T. Mannel, N. Offen, and Y. M. Wang, Phys. Rev. **D83**, 094031 (2011), 1103.2655.
[37] A. Bharucha, JHEP **05**, 092 (2012), 1203.1359.
[38] I. Sentitemsu Imsong, A. Khodjamirian, T. Mannel, and D. van Dyk, JHEP **02**, 126 (2015), 1409.7816.
[39] I. I. Y. Bigi, M. A. Shifman, N. G. Uraltsev, and A. I. Vainshtein, Phys. Rev. **D52**, 196 (1995), hep-ph/9405410.
[40] A. Kapustin, Z. Ligeti, M. B. Wise, and B. Grinstein, Phys. Lett. **B375**, 327 (1996), hep-ph/9602262.
[41] P. Gambino, T. Mannel, and N. Uraltsev, Phys. Rev. **D81**, 113002 (2010), 1004.2859.
[42] P. Gambino, T. Mannel, and N. Uraltsev, JHEP **10**, 169 (2012), 1206.2296.
[43] R. Aaij et al. (LHCb), Nature Phys. **11**, 743 (2015), 1504.01568.
[44] R. Aaij et al. (LHCb), Phys. Rev. **D96**, 112005 (2017), 1709.01920.
[45] W. Detmold, C. Lehner, and S. Meinel, Phys. Rev. **D92**, 034503 (2015), 1503.01421.
[46] C. M. Bouchard, G. P. Lepage, C. Monahan, H. Na, and J. Shigemitsu, Phys. Rev. **D90**, 054506 (2014).
[47] C. J. Monahan, H. Na, C. M. Bouchard, G. P. Lepage, and J. Shigemitsu, Phys. Rev. **D95**, 114506 (2017), 1703.09728.
[48] A. Bazavov et al. (MILC), Rev. Mod. Phys. **82**, 1349 (2010).
[49] C. Bernard (MILC), Phys. Rev. **D65**, 054031 (2002), hep-lat/0111051.
[50] H. Na, C. J. Monahan, C. T. Davies, R. Horgan, G. P. Lepage, and J. Shigemitsu, Phys.Rev. **D86**, 034506 (2012).
[51] C. Monahan, J. Shigemitsu, and R. Horgan, Phys.Rev. **D87**, 034017 (2013).
[52] H. Na, C. T. Davies, E. Follana, G. P. Lepage, and J. Shigemitsu, Phys.Rev. **D82**, 114506 (2010).
[53] Lepage, G.P., lsqfit v4.8.5.1, URL `https://doi.org/10.5281/zenodo.10236`.
[54] Lepage, G.P., corrfitter v3.7.1, URL `https://doi.org/10.5281/zenodo.10237`.
[55] H. Na, C. T. Davies, E. Follana, J. Koponen, G. P. Lepage, et al., Phys.Rev. **D84**, 114505 (2011).
[56] C. Bouchard, G. P. Lepage, C. Monahan, H. Na, and J. Shigemitsu (HPQCD), Phys. Rev. Lett.

111, 162002 (2013), [Erratum: Phys. Rev. Lett.112,no.14,149902(2014)].
[57] C. Bouchard, G. P. Lepage, C. Monahan, H. Na, and J. Shigemitsu (HPQCD), Phys. Rev. **D88**, 054509 (2013), [Erratum: Phys. Rev.D88,no.7,079901(2013)].
[58] C. Bourrely, I. Caprini, and L. Lellouch, Phys. Rev. **D79**, 013008 (2009), [Erratum: Phys. Rev.D82,099902(2010)].
[59] E. B. Gregory, C. T. H. Davies, E. Follana, E. Gamiz, I. D. Kendall, G. P. Lepage, H. Na, J. Shigemitsu, and K. Y. Wong, Phys. Rev. Lett. **104**, 022001 (2010).
[60] J. Bijnens and I. Jemos, Nucl. Phys. **B840**, 54 (2010), [Erratum: Nucl. Phys.B844,182(2011)], 1006.1197.
[61] J. Bijnens and I. Jemos, Nucl. Phys. **B846**, 145 (2011), 1011.6531.
[62] V. Lubicz, L. Riggio, G. Salerno, S. Simula, and C. Tarantino, PoS **LATTICE2016**, 280 (2016), 1611.00022.
[63] J. P. Lees et al. (BaBar), Phys. Rev. Lett. **109**, 101802 (2012).
[64] J. P. Lees et al. (BaBar), Phys. Rev. **D88**, 072012 (2013).
[65] M. Huschle et al. (Belle), Phys. Rev. **D92**, 072014 (2015).
[66] Y. Amhis et al. (HFAG), Average of $R(D)$ and $R(D^*)$ (2016), URL `https://www.slac.stanford.edu/xorg/hfag/semi/eps15/eps15_dtaunu.html`.
[67] J. F. Kamenik and F. Mescia, Phys. Rev. **D78**, 014003 (2008).
[68] J. A. Bailey, A. Bazavov, C. Bernard, C. Bouchard, C. DeTar, et al., Phys.Rev. **D85**, 114502 (2012).